crystals

MDPI

Article

High-Temperature Tribological Behavior of Fast-Hot-Pressed NiCr/Cr_3C_2-LaF_3 Self-Lubrication Composite

Hao Yang [1,2], Chuanbing Huang [1,2,3,*], Haozhong Lv [3,4], Yongjun Liu [1,2], Yonghui Sun [3], Huifeng Zhang [1,2,3], Hao Lan [1,2,3], Yang Wu [1,2] and Weigang Zhang [1,2,3,4]

1 School of Rare Earths, University of Science and Technology of China, Hefei 230026, China; yanghao77@yeah.net (H.Y.); 17318588230@163.com (Y.L.); hfzhang@ipe.ac.cn (H.Z.); hlan@gia.cas.cn (H.L.); wu17379102769@163.com (Y.W.); wgzhang@ipe.ac.cn (W.Z.)
2 Ganjiang Innovation Academy, Chinese Academy of Sciences, Ganzhou 341119, China
3 Institute of Process Engineering, Chinese Academy of Sciences, Beijing 100190, China; hzlv@ipe.ac.cn (H.L.); yhsun@ipe.ac.cn (Y.S.)
4 School of Chemical Engineering, University of Chinese Academy of Sciences, Beijing 100049, China
* Correspondence: cbhuang@gia.cas.cn

Abstract: This article details a method for preparing cermet matrix composites via Fast hot pressing (FHP) sintering technology and emphasizes their potential use in extremely high-temperature settings. The material primarily consists of NiCr alloy, Cr_3C_2, and LaF_3. An in-depth investigation was conducted on the tribological properties of the specimen by conducting sliding tests against a Si_3N_4 ball at varying temperatures, including room temperature (RT), 400 °C, 600 °C, and 800 °C. Advanced techniques such as scanning electron microscopy, micro-XRD, and micro-Raman spectroscopy were employed to examine the friction surfaces formed under different frictional temperatures. The findings reveal a uniform composition and high density within the composites. It is noteworthy that as the LaF_3 content increases, the hardness of the ceramic phase diminishes. Conversely, the hardness of the alloy phase augments with the addition of LaF_3, provided that its content remains below 15 wt%. The composite material containing 15 wt% LaF_3 demonstrates superior hardness values, with the ceramic phase reaching HV1412 and the alloy phase achieving HV384. Furthermore, the coefficient of friction of the composite material was evaluated. The coefficient of friction of the composite is between 0.74 and 0.4 and the wear rate is 4.46×10^{-6}–5.72×10^{-5} $mm^3N^{-1}m^{-1}$ from room temperature to 800 °C. The lubrication behavior at low temperature is mainly attributed to the lubricating effect of LaF_3, and at high temperature it is due to the tribochemical reaction to form $LaCrO_3$ with good lubricating properties, which plays a synergistic lubricating role with Cr_2O_3.

Keywords: high temperature; self-lubrication; LaF_3; NiCr/Cr_3C_2

Citation: Yang, H.; Huang, C.; Lv, H.; Liu, Y.; Sun, Y.; Zhang, H.; Lan, H.; Wu, Y.; Zhang, W. High-Temperature Tribological Behavior of Fast-Hot-Pressed NiCr/Cr_3C_2-LaF_3 Self-Lubrication Composite. *Crystals* **2024**, *14*, 365. https://doi.org/10.3390/cryst14040365

Academic Editor: Benilde F. O. Costa

Received: 19 March 2024
Revised: 4 April 2024
Accepted: 9 April 2024
Published: 12 April 2024

1. Introduction

As science and technology progress relentlessly, especially in the high-end equipment manufacturing and cutting-edge industries, there has been a marked increase in the energy density between mechanical surfaces. This escalation has led to a considerable rise in material service temperatures, often culminating in premature wear and failure. As service time extends or operating temperatures increase, the reliability of conventional wear-resistant materials gradually diminishes. The adoption of further component optimization designs aimed at directly enhancing the material's overall friction performance could offer a novel material option for the hot-end components of advanced equipment. To tackle this challenge effectively, there is an urgent need for the development of materials that exhibit both exceptional wear resistance and self-lubricating characteristics, particularly at elevated temperatures. This represents a critical research focus in contemporary materials science [1–3]. For applications that demand such stringent requirements, materials must possess not only lubrication and wear resistance but also exhibit robust

oxidation and corrosion resistance. Cermet composites have demonstrated remarkable efficacy in addressing these challenges. Among these superior materials, NiCr/Cr_3C_2 matrix composites hold a prominent position [4–7]. In the 1990s, Duran and colleagues made a groundbreaking discovery that the liquid-phase sintering process could yield nearly fully dense NiCr/Cr_3C_2 metal ceramics with a carbide content ranging from 75 to 95 wt% in just 15 min at a relatively low temperature of 1300 °C. Furthermore, these metal ceramics possess favorable mechanical properties, making them highly suitable for demanding applications [8]. The remarkable wear resistance of this material system has sparked extensive research and application in various fields, including industrial production and advanced equipment. Rahul and co-workers produced NiCr/Cr_3C_2 coatings through plasma spray, detonation spray (DS), high velocity oxy-fuel (HVOF), and high velocity air-fuel spray (HVAF) techniques. Their evaluation of the coatings' corrosion resistance concluded that they were well-suited for boiler protection [9]. Zhang and his team employed supersonic atmospheric plasma spraying (SAPS) to create NiCr/Cr_3C_2 coatings and investigate their corrosion and wear resistance. They observed improvements after sealing treatment in simulated underground coal mine environments, marked by reduced corrosion current and wear rate [10]. Hu and his colleagues achieved the fabrication of microcrystalline Cr_3C_2 and amorphous SiO_2-reinforced NiCr composites, which exhibited high ductility, a yield strength of 449 MPa, ultimate tensile strength of 838 MPa, and ductility of 20.5% [11]. Yang and his group utilized high-speed oxygen fuel spraying (HVOF) to deposit a novel micro-nano-structured Cr_3C_2-NiCr metal ceramic coating on 316 L stainless steel, achieving low porosity of 0.34% or less and high microhardness of at least $1105HV_{0.3}$ [12]. Despite the numerous advantages offered by the NiCr/Cr_3C_2 material system, its lubrication performance remains inadequate. This limitation becomes particularly apparent at elevated temperatures, where the high friction coefficient can lead to exacerbated wear during the friction process. To overcome this limitation, researchers often incorporate solid lubricants into the material system to enhance its lubrication properties [13].

Fluorine-based solid lubricants have gained widespread recognition for their remarkable performance across a broad temperature spectrum, as well as their outstanding chemical and thermal stability. These qualities make them particularly suitable for high-temperature applications in various materials [2]. The low shear strength of fluorides is a key factor that contributes to their effectiveness as lubricants. During the friction process, this low shear strength facilitates a brittle-to-ductile transformation, allowing the lubricants to spread evenly across the surface of contact. This, in turn, creates a thin film that significantly reduces the friction coefficient, leading to enhanced friction reduction. NASA's early research on fluorides provides compelling evidence of this phenomenon. [14–16]. Common fluoride compounds utilized as lubricants include CaF_2, BaF_2, and certain rare earth fluorides. In recent studies, researchers have explored the use of these fluorides in various composite materials. For instance, Zhao and colleagues successfully prepared Cr_3C_2–NiCr–Mo–BaF_2 composites using the spark plasma sintering technique. The incorporation of Mo and BaF_2 resulted in a remarkably low friction coefficient of 0.27 at 900 °C [17]. Kotkowiak and co-workers fabricated a nickel-based composite containing 20% CaF_2 using powder metallurgy and conducted a comprehensive study on the lubrication mechanism of CaF_2 at temperatures ranging from 200 to 600 °C [18]. Su et al. produced an Ag-BaF_2·CaF_2-Cr_3C_2-NiCr composite coating through high-velocity oxygen fuel (HVOF) spraying. Their findings indicated that the combination of BaF_2·CaF_2 and Ag effectively enhances tribological performance across a wide temperature range. The formation of chromates at elevated temperatures plays a crucial role in improving friction behavior [19]. These studies have demonstrated that fluoride has excellent lubrication effects. The excellent lubrication effects of rare earth fluorides such as CeF_3 and LaF_3, have been extensively documented. These compounds possess a unique layered hexagonal crystal structure that contributes to their superior lubricating properties. NASA's Sliney conducted a preliminary investigation into the tribological behavior of these fluorides, revealing that both LaF_3 and CeF_3 can significantly reduce the friction coefficient of materials in both air and argon

atmospheres [20]. Furthermore, Lu and colleagues incorporated CeF_3 into a Ni-based alloy and observed its effective anti-friction properties [21]. Similarly, Ren et al. augmented cobalt-based composites with LaF_3 and CeO_2, noting that the introduction of these rare earth compounds facilitated chromate formation during high-temperature friction. This led to a significant reduction in both the friction coefficient and material wear at elevated temperatures [22]. Multiple studies have also highlighted the ability of LaF_3 to enhance the formation of frictional transfer films in polytetrafluoroethylene (PTFE)-based composites [23,24]. Despite the considerable amount of research that has been devoted to exploring the lubricating properties of LaF_3, a challenge arises in isolating its specific effects. This difficulty stems from the common practice of utilizing LaF_3 in combination with a range of other lubricating materials. Consequently, disentangling its individual contribution to the overall lubrication process poses a significant analytical hurdle. Furthermore, there exists a notable dearth of studies focusing on the lubrication mechanism of LaF_3, especially within the context of high-temperature ceramic–metal friction systems. In light of these gaps in the existing literature, the present study prioritizes LaF_3 as the primary lubricating material. Its aim is twofold: to facilitate the development of materials that exhibit superior friction performance and to contribute to filling the aforementioned research voids in this field.

2. Materials and Methods

2.1. Preparation of Composites

This study successfully synthesized NiCr/Cr_3C_2-based composite materials with LaF_3 concentrations of 0 wt%, 10 wt%, 15 wt%, and 20 wt% using a fast hot pressing sintering method of powder metallurgy, maintaining a constant mass ratio of NiCr to Cr_3C_2 at 1:3. The mass ratio of Ni to Cr in the NiCr alloy was 4:1. These materials were designated as NCL0, NCL10, NCL15, and NCL20, respectively. Commercially available NiCr alloy powder, Cr_3C_2 powder, and LaF_3 powder with particle sizes finer than 325 mesh were utilized as the raw materials. Initially, a high-energy ball milling process was employed to mix NiCr alloy powder, Cr_3C_2 powder, and LaF_3 powder in a ball mill for 12 h. The ball-to-material ratio was maintained at 10:1, and anhydrous ethanol was used as the milling medium. Subsequently, the milled powder was evaporated using rotary evaporation. The prepared composite powder was then placed into a graphite mold. After evacuating the furnace to a pressure below 5 Pa, high-purity argon gas was introduced to safeguard the sample. The temperature was gradually increased to 1100 °C at a rate of 100 °C/min, while maintaining a constant pressure of 50 MPa for a duration of 5 min. Subsequently, the sintered samples were cooled to room temperature within the furnace. The cooled samples were then uniformly polished and smoothed using sandpaper in preparation for subsequent tests.

2.2. Characterization

The phase composition of the composite material was examined utilizing an X'Pert PRO MPD X-ray diffractometer (Panaco Analytical Instruments, Almelo, Netherlands) within a 2θ range spanning from 15 to 80°. The microstructure, along with the morphology of both the composite materials and their wear scar surfaces, were scrutinized using a Gemini 300 scanning electron microscope (SEM) (Zeiss, Oberkochen, Germany) equipped with an Ultim MAX energy-dispersive spectrometer (EDS). Furthermore, the three-dimensional morphology of the wear surface, including its interface, underwent observation and analysis via Nexview white light interference microscopy. Lastly, the phase composition of the wear scar was investigated through the employment of an inVia confocal Raman spectrometer and a Rigaku SmartLab SE micro-XRD instrument.

The densities and porosities of the composites were quantified utilizing the Archimedes drainage method. Each specimen underwent a minimum of three trials, and the corresponding mean values are presented in Table 1. Furthermore, the Vickers hardness of the composite materials was determined using the HX1000-TM micro-Vickers hardness tester (Shanghai Optical Instrument Factory, Shanghai, China), with a ceramic phase load

of 300 g, a metal phase load of 100 g, and a holding time of 15 s. The frictional properties of the composite materials were assessed using the HT-1000 high-temperature friction (Lanzhou Zhongke Kaihua Technology Development Co., Ltd, Lanzhou, China) and wear testing machine. The cross-sectional view of the equipment is depicted in Figure 1. Prior to the testing, the sample was thoroughly cleaned and dried with acetone. A Si_3N_4 ball, measuring 6 mm in diameter and possessing a hardness of 1700 HV, served as the grinding ball. The testing parameters included a load of 1 kg, a rotational speed of 365 r/min, a rotation diameter of 5 mm, and a test duration of 20 min.

Table 1. Composition, density, and porosity of composites.

Material	Composition(wt%)			Density ($g \cdot cm^{-3}$)	Porosity (%)
	80Ni-20Cr	Cr_3C_2	LaF_3		
NCL0	25.00	75.00	0.00	6.93 ± 0.02	0.30 ± 0.15
NCL10	21.82	68.18	10.00	6.71 ± 0.08	0.16 ± 0.15
NCL15	19.78	65.22	15.00	6.74 ± 0.01	0.10 ± 0.13
NCL20	17.50	62.50	20.00	6.67 ± 0.02	0.56 ± 0.26

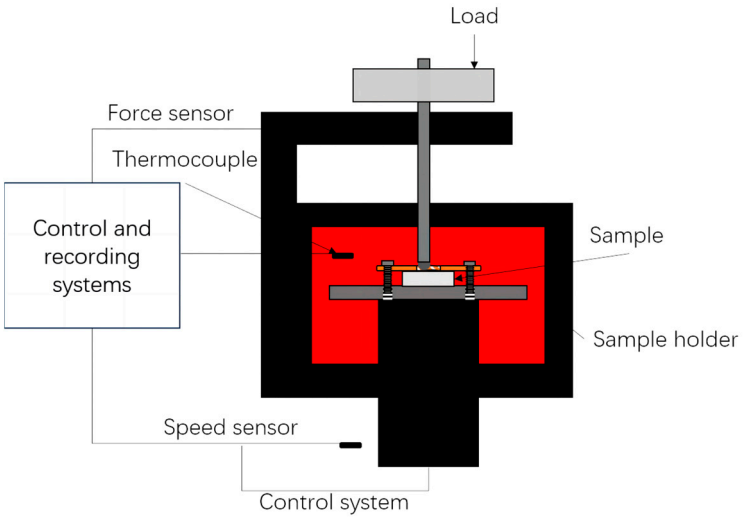

Figure 1. Schematic diagram of the cross-section of the friction and wear machine.

3. Results and Discussion

3.1. Microstructure and Mechanical Properties

The X-ray diffraction (XRD) images depicting both the pre-sintered powder and the post-sintered bulk of the composite material are presented in Figure 2. Prior to the sintering process, the NiCr/Cr_3C_2 powder consists predominantly of NiCr and Cr_3C_2 phases. The NiCr/Cr_3C_2-LaF_3 powder comprises additional LaF_3 phases alongside NiCr and Cr_3C_2. This observation concurs with the initial design specifications and provides evidence that the powder maintains its compositional integrity, remaining relatively stable and free from oxidation during the ball milling process. Upon sintering, the resulting bulk material exhibits a phase composition that closely resembles that of the original powder. This indicates that no significant chemical reactions occurred during the fast hot pressing sintering process. Notably, this method differs from traditional liquid-phase sintering or hot pressing sintering techniques in that it utilizes direct current to expedite the shaping of materials. This innovative approach reduces both the holding time and the sintering temperature, thereby preserving the material's original composition more effectively and mitigating the likelihood of undesirable chemical reactions during sintering. This approach preserves the material's composition more effectively and prevents chemical reactions during sintering. A detailed comparison of the pre- and post-sintered materials reveals that the phase composition remains largely unchanged throughout the sintering process.

However, the diffraction peaks of the sintered composite exhibit a notable intensification, indicating enhanced crystallinity [25]. As illustrated in Figure 2b, the introduction of LaF_3 results in a distinct broadening of the diffraction peaks associated with the Cr_3C_2. This broadening is primarily attributed to the grain refining effect of lanthanum (La), a rare earth element known to refine grains and enhance inter-grain exchange coupling, as evidenced by previous studies [26–28]. Grain refinement is a desirable outcome that can potentially improve the mechanical and physical properties of the sintered composite.

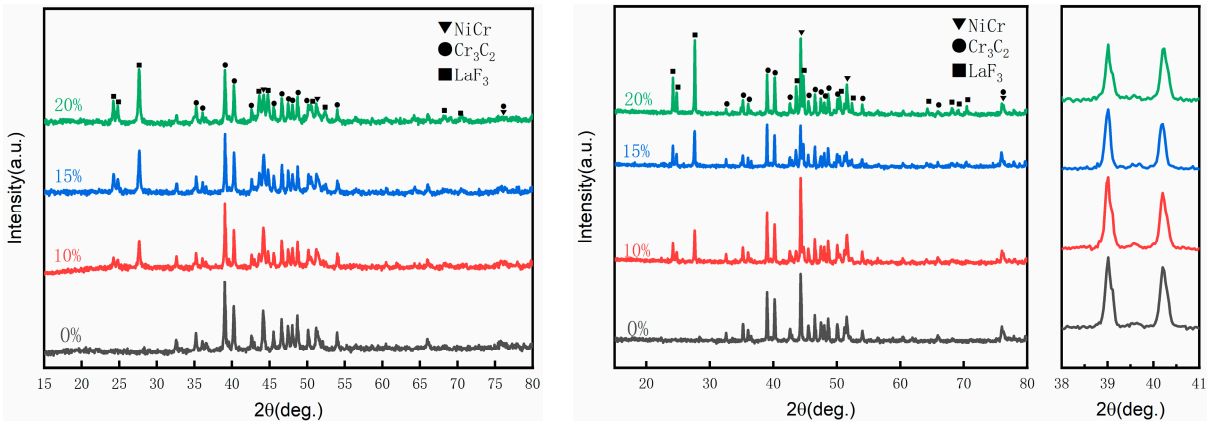

Figure 2. XRD patterns of composites before (**a**) and after (**b**) FHP.

Figure 3 displays scanning electron microscope images of the composite. Based on the graph, it is evident that NCL0 exhibits two distinct features, whereas NCL10-NCL20 displays three. These features share similar characteristics: the darkest contrast is attributed to the Cr_3C_2 phase, the moderately dark gray area represents the NiCr phase, and the lightest region corresponds to the LaF_3 phase. Cr_3C_2 constitutes a continuous ceramic phase. Simultaneously, LaF_3 nanoparticles are homogeneously distributed within the Cr_3C_2 phase. The addition of LaF_3 is evident in the density variations presented in Table 1, facilitating the sintering of the bulk material. The NiCr alloy is uniformly distributed throughout the bulk in a droplet-like form. Fast hot pressing sintering [29–31] enhances the sintering activity of Cr_3C_2 powder, enabling dense sintering at 1100 °C. Furthermore, the presence of the NiCr alloy phase significantly reduces porosity, resulting in a nearly fully dense block. Given this composite structure, we categorize its hardness into two distinct phases: a ceramic phase primarily composed of Cr_3C_2 and LaF_3, and a metal phase primarily constituted of the NiCr alloy. Figure 4a shows that as the amount of LaF_3 increases, the Vickers hardness of the ceramic phase decreases. In particular, when the addition amount reaches 20 wt%, the Vickers hardness of the ceramic phase decreases sharply, which is mainly due to the low hardness of LaF_3 itself, but thanks to the high density of the bulk material, LaF_3 can still have the high hardness of the ceramic phase of 1412 HV when added to 15%. Figure 4b displays that the Vickers hardness of the alloy phase increases proportionally with the addition of LaF_3 up to a concentration of 15 wt%. However, it experiences a rapid decrease when the LaF_3 content reaches 20 wt%. This hardness trend aligns with the porosity variation pattern observed in these materials.

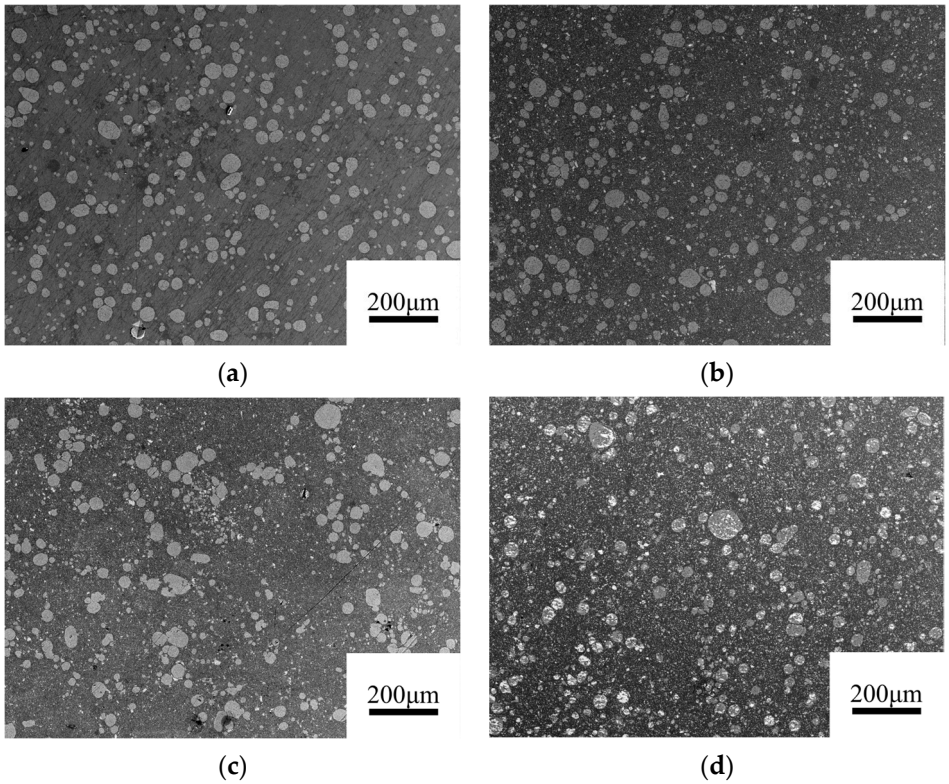

Figure 3. SEM images: (**a**) NCL0; (**b**) NCL10; (**c**) NCL15; (**d**) NCL20.

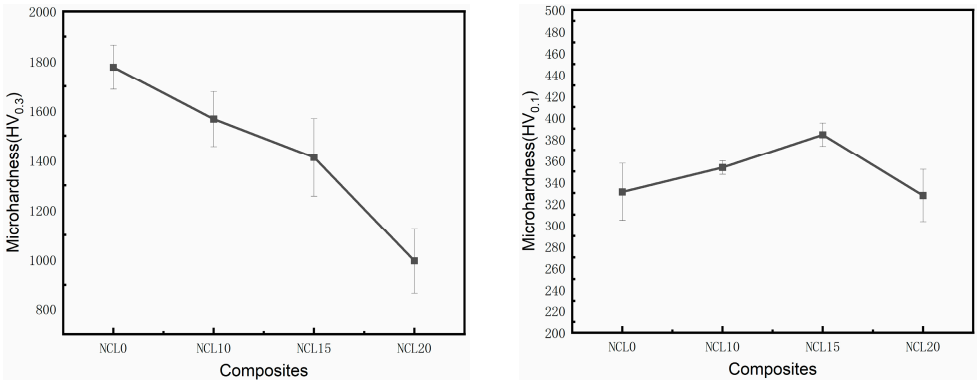

Figure 4. Ceramic-phase (**a**) and metallic-phase (**b**) Vickers hardness of composites.

3.2. Tribological Properties of the Composites

Figure 5 exhibits the frictional characteristics of the composite material at varying temperatures and under countergrinding with a Si_3N_4 ball. Notably, composite blocks fabricated via the FHP method possess superior wear resistance, primarily attributed to their elevated hardness and density. With the exception of 600 °C, the friction coefficient of composite materials exhibits a downward trend as the friction temperature increases. Furthermore, the wear amount increases from room temperature to 600 °C and exhibits variations at 800 °C, influenced by diverse LaF_3 addition amounts. These variations are influenced by various factors, including oxidation, component sublimation, and the in situ formation of novel substances during the friction process. Overall, the frictional behavior of the composites is enhanced at most temperatures upon the addition of LaF_3. Notably, NCL15 attains a relatively low wear rate of 3.85×10^{-6} $mm^3N^{-1}m^{-1}$ at room temperature, whereas NCL20 exhibits the lowest friction coefficient.

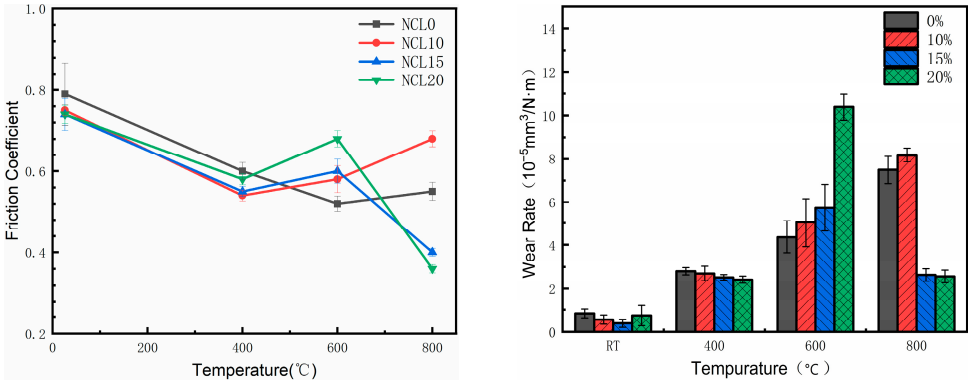

(**a**) (**b**)

Figure 5. Friction coefficients (**a**) and wear rates (**b**) of the NCL0, NCL10, NCL15, and NCL20 composites at different temperatures.

Figure 6 demonstrates the temporal variation in the coefficient of friction for various composite materials during the high-temperature friction test. Notably, the sample containing LaF_3 exhibits minimal fluctuations in the friction coefficient across all temperatures and attains a stable state shortly after the commencement of tribological testing. Conversely, as depicted in Figure 6a, the NCL0 sample devoid of LaF_3 displays significant fluctuations in the friction coefficient and maintains a consistent upward trend towards the conclusion of the experiment. For instance, towards the end of the experiment at room temperature, its friction coefficient surges to approximately 0.9.

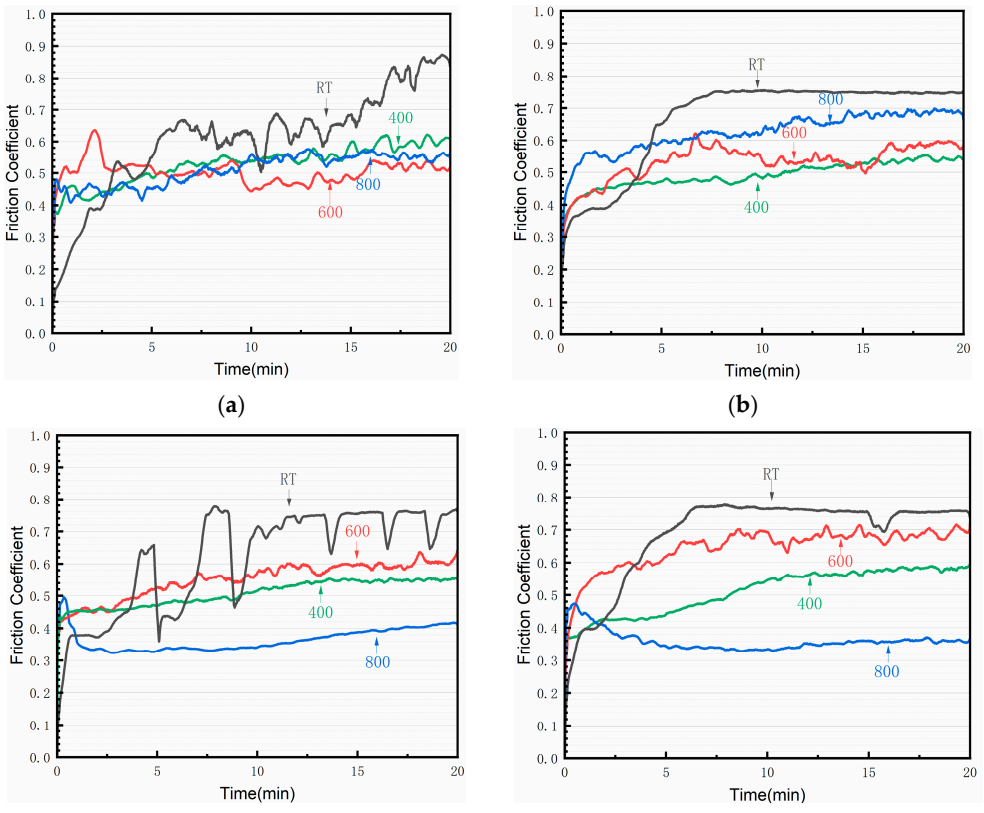

(**a**) (**b**)

(**c**) (**d**)

Figure 6. Friction coefficient curves: (**a**) NCL0; (**b**) NCL10; (**c**) NCL15; (**d**) NCL20.

Despite having the lowest friction coefficient and wear amount at 800 °C, NCL20 exhibits the highest friction coefficient and wear amount at 600 °C. Consequently, the

results presented in Figures 5 and 6 clearly indicate that NCL15 material demonstrates superior friction properties across a wide temperature range, making it a more favorable choice overall.

3.3. Morphologies and Constituents of Worn Surfaces

To better understand the relationship between the wear mechanism and tribological properties of various composite materials under frictional conditions, we conducted a microstructural analysis of the wear marks using scanning electron microscopy (SEM), X-ray diffraction (XRD), micro-XRD, and micro-Raman spectroscopy. Figure 7 depicts the topographical features of the composite's wear surface, spanning from room temperature to 800 °C, while Figure 8 illustrates the three-dimensional topography of these wear marks. Figures 9 and 10 show the elemental distribution of the wear marks of NCL20 and NCL0 after friction at 400 °C, 600 °C and 800 °C, respectively Inspection of Figures 7a and 8a reveals that the composite material exhibits increased hardness at room temperature, resulting in shallow wear marks. The abrasive particles on the surface are more pronounced, indicating a predominance of abrasive and fatigue wear mechanisms. In comparison to other composites, NCL0 exhibits a higher concentration of grinding chips and pits on the wear marks' surface. Furthermore, Figure 8a demonstrates that the wear marks of NCL0, subjected to friction at room temperature, exhibit numerous furrows. During the friction process, Cr_3C_2 particles detach from the friction interface and become interspersed between the two friction surfaces, continuously generating a small amount of cutting and contributing to the formation of a transfer film. Consequently, the friction coefficient of NCL0 at room temperature is elevated.

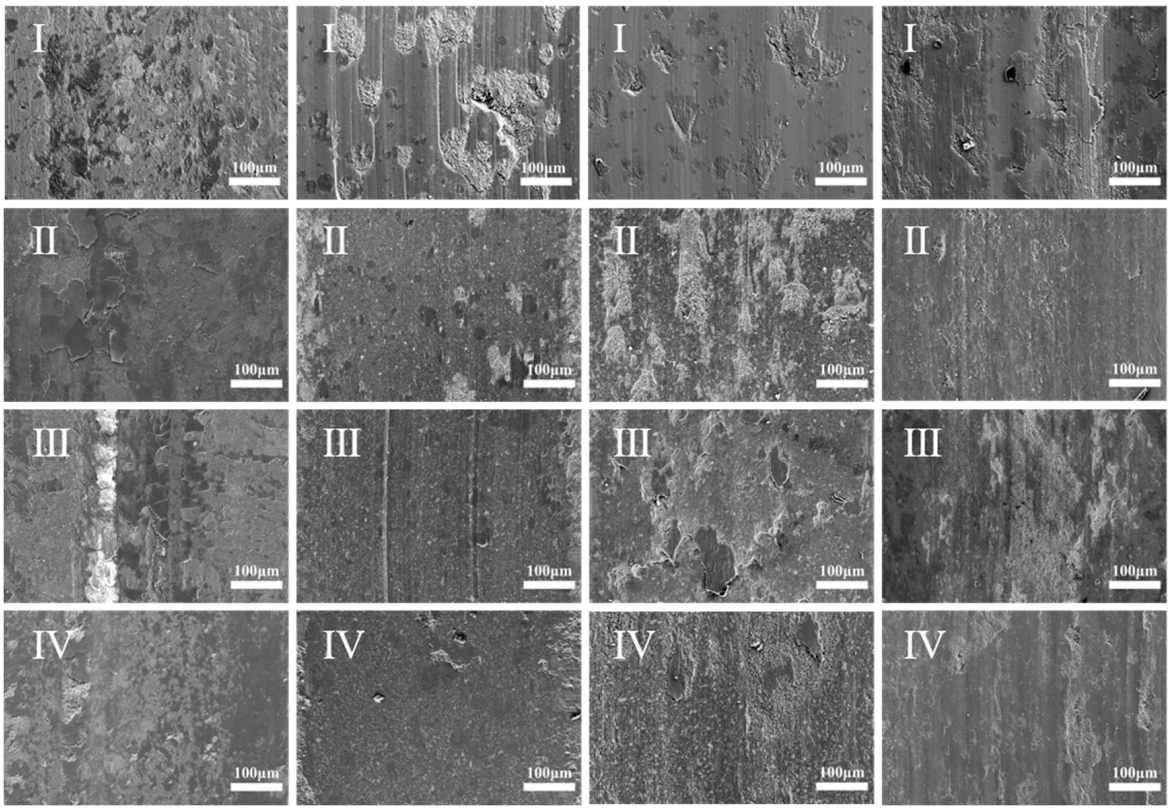

Figure 7. SEM micrographs of the worn surfaces of NCL0 (I), NCL10 (II), NCL15 (III), and NCL120 (IV) composites tested at room temperature (**a**), 400 °C (**b**), 600 °C (**c**), and 800 °C (**d**).

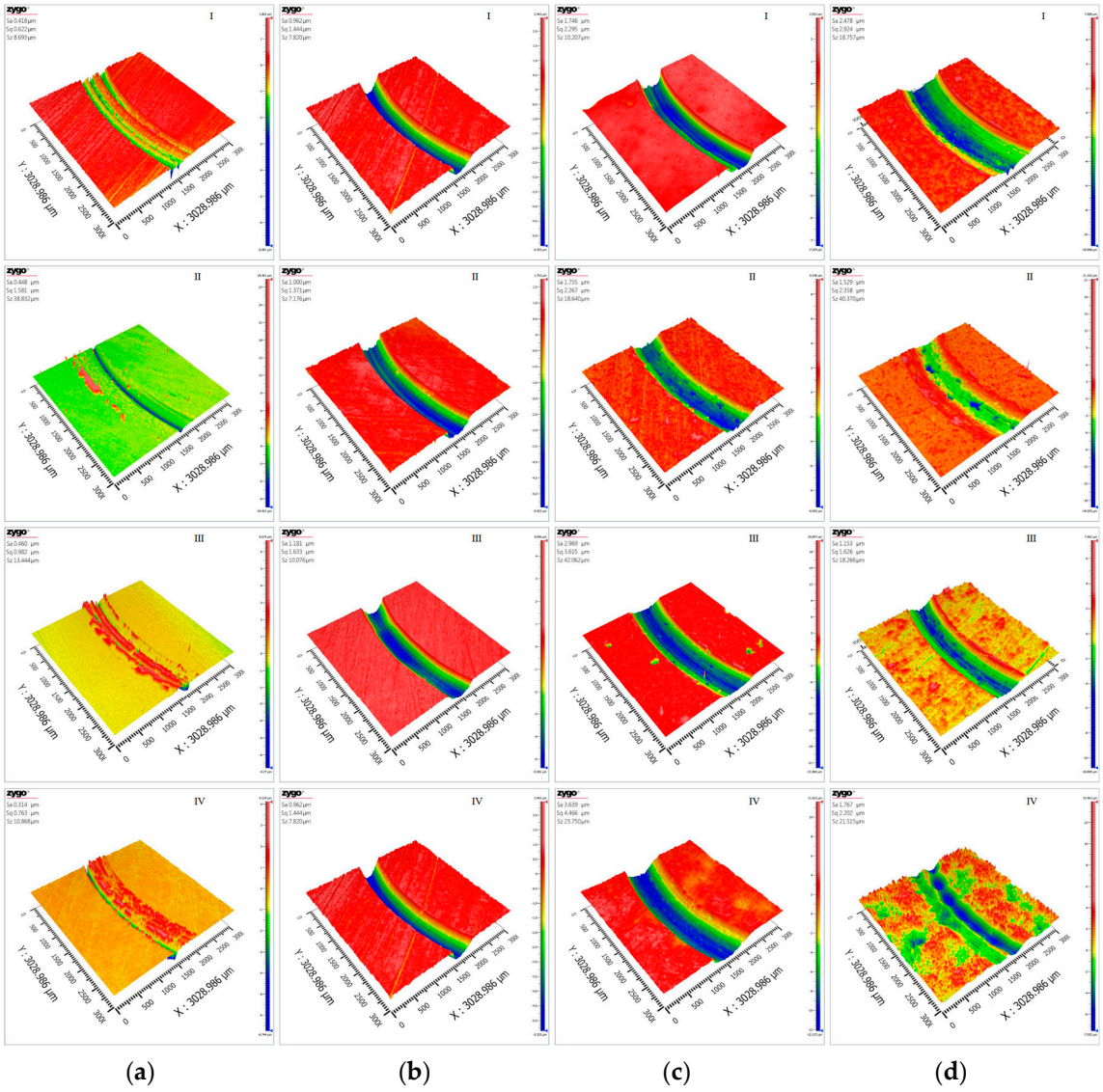

Figure 8. The 3D surface topography of the worn surfaces of NCL0 (I), NCL10 (II), NCL15 (III), and NCL20 (IV) composites tested at room temperature (**a**), 400 °C (**b**), 600 °C (**c**), and 800 °C (**d**).

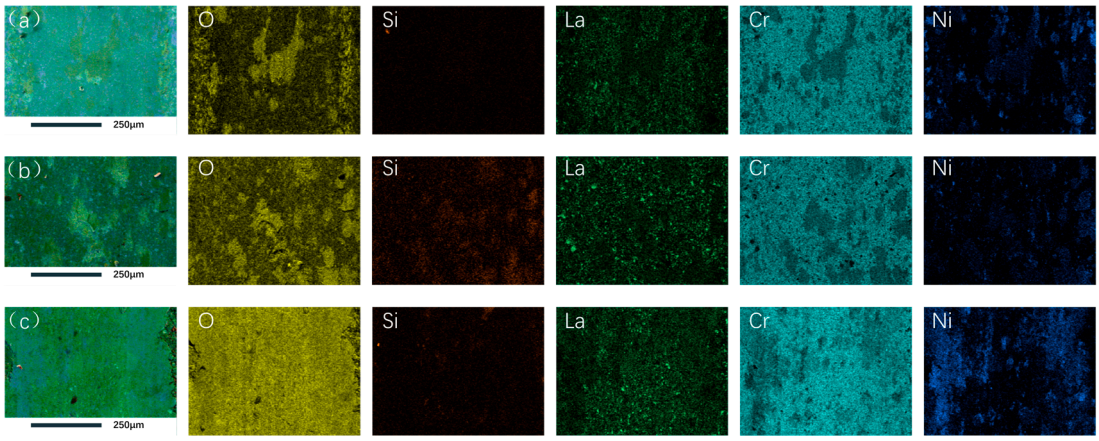

Figure 9. EDS mappings of the worn cross-sections of the NCL20 at 400 °C (**a**), 600 °C (**b**), and 800 °C (**c**).

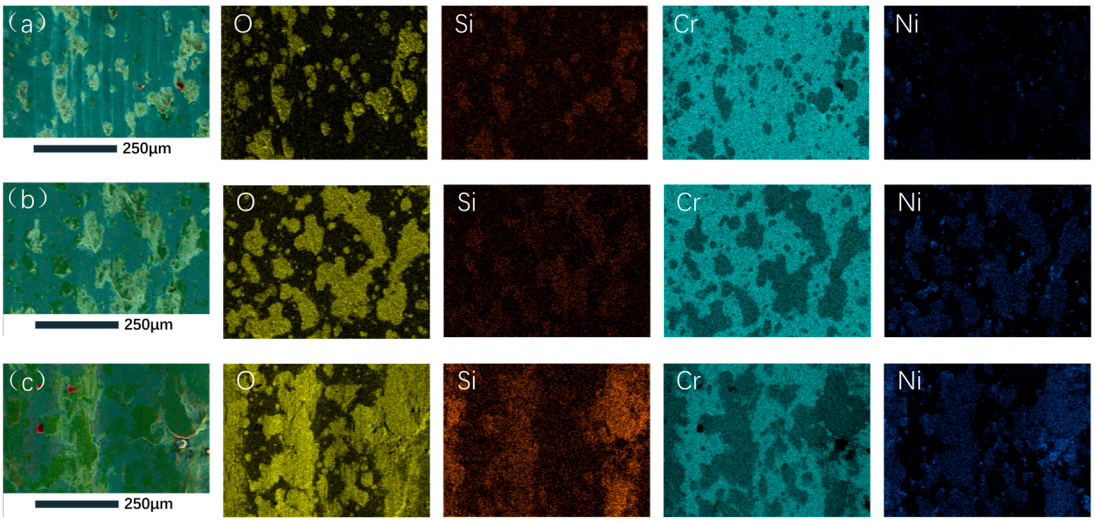

Figure 10. EDS mappings of the worn cross-sections of the NCL0 at 400 °C (**a**), 600 °C (**b**), and 800 °C (**c**).

Upon analyzing Figures 7b and 8b, it becomes evident that the abrasive particles on the surface of the LaF_3-reinforced composite material decrease and assume a smoother texture as the temperature rises to 400 °C. Exposure to a high-temperature environment coupled with frictional stress facilitates the diffusion, precipitation, and enrichment of LaF_3 on the friction surface, thus generating a lubricating film. Additionally, Figure 9a corroborates the even distribution of La elements on the friction surface. Conversely, the absence of LaF_3 abrasion in NCL0 results in numerous pits and abrasion debris, attributed primarily to the material's limited plasticity and lubrication deficiency. These pits at the friction interface progressively develop into deeper, scaly formations during movement, thereby maintaining a comparatively high friction coefficient and wear rate. Similarly, Figure 8b illustrates the wear patterns observed on NCL0.

When the friction temperature increases to 600 °C, Figure 7c reveals the emergence of numerous oxides on the material's surface. Furthermore, oxidation leads to peeling off of the LaF_3-reinforced composite material's surface, suggesting that the oxidation products are insufficient for forming a dense oxide film examination of the wear marks; analysis reveals the presence of peeling debris resulting from oxidation wear, along with a small, compacted glaze layer. Nevertheless, this layer's minimal size and the continuous abrasion caused by hard Cr_3C_2 particles negate any potential improvement in friction performance. Conversely, in the absence of LaF_3, the peeling of Cr_3C_2 is less severe, accompanied by the softening of the NiCr alloy and a subsequent decrease in the friction coefficient. Additionally, Figure 8b illustrates that the composite material with LaF_3 attains its peak volume wear at this frictional temperature. The wear marks of the composite material with LaF_3 added reached the highest level in both width and depth at this temperature. Figure 9b demonstrates that the oxide layer on the NCL20 wear mark rubbed at 600 °C is discontinuous and not dense enough. When the friction temperature reaches 800 °C, numerous deep grooves and an uneven distribution of components are still observed on the NCL0 wear mark surface.As can be seen from Figure 10c, the oxide layer on the surface of the NCL0 wear mark is not continuous and is distributed in sheets. In contrast, the surface of the wear mark with LaF_3 added begins to densify. Notably, a transfer film of composite oxides covers the surface, with the NCL15 and NCL20 transfer films appearing particularly dense. Only minor plowing is visible on the friction surface, indicating some micro-plowing occurred during the friction process. However, the glaze layer of NCL10 displays numerous fine debris and pores, which offer inadequate protection. Figure 9c further reveals that the oxygen distribution on the NCL20 friction surface is completely dense at 800 °C, with metal elements such as Cr, La, and Ni uniformly distributed. This

suggests that the surface comprises a dense composite oxide layer, resulting in a lower friction coefficient and wear rate.

In order to comprehensively understand the phase transition process occurring during high-temperature friction of materials, XRD tests were conducted on each sample following friction experiments conducted at temperatures of 400 °C, 600 °C, and 800 °C. The results are presented in Figure 11. The analysis reveals that as the temperature rises and friction progresses, grains of certain components undergo notable changes, characterized by a narrowing of the diffraction peak's half-peak width and an increase in peak intensity [25]. Notably, at 400 °C, low-intensity Cr_3O_2 diffraction peaks emerged in all samples, with their intensities increasing as the temperature rose. Furthermore, composites containing LaF_3 began to produce LaOF at 600 °C, potentially explaining the deterioration in friction behavior observed at this temperature [20]. Zhu et al.'s study demonstrates that annealing LaF_3 at 500 °C for a specified duration results in its transformation into LaOF [32], a phenomenon that is also observed during friction at this temperature. This oxidation process of LaF_3 initiates the detachment of Cr_3C_2 hard particles, ultimately leading to the loss of hard phase support on the friction surface and consequently enhancing wear.

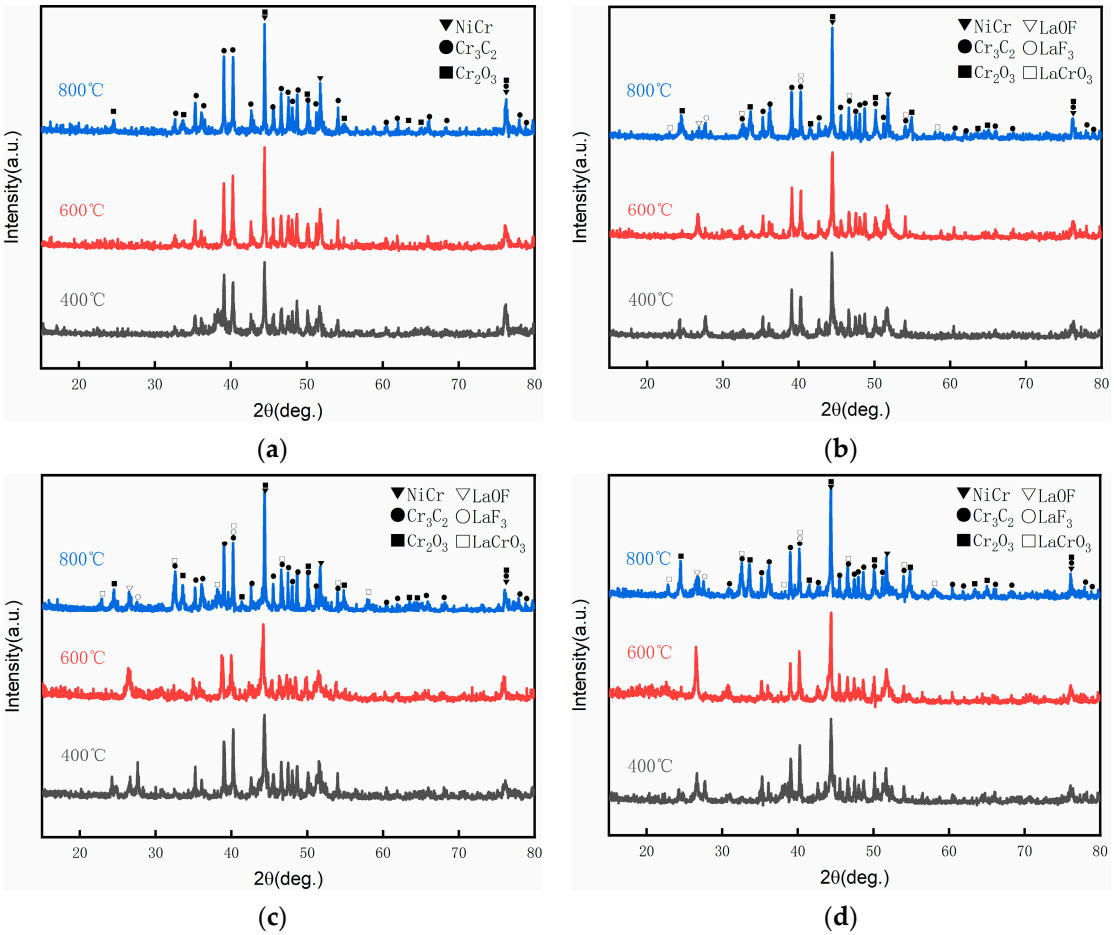

Figure 11. XRD patterns of (**a**) NCL0, (**b**) NCL10, (**c**) NCL15, and (**d**) NCL20 composites after friction at 400~800 °C.

To further investigate the formation of oxides during the friction process, micro-area XRD and micro-Raman testing were conducted on the worn surfaces of NCL0 and NCL20. As illustrated in Figure 12, micro-XRD patterns of the wear scars on NCL0 and NCL20 reveal the presence of oxides, predominantly NiO, Cr_2O_3, LaOF, and $LaCrO_3$ [17,32,33]. These oxides closely resemble the phase composition of the bulk material. It is evident that, contrary to XRD testing performed on the entire block, NCL20 does not exhibit any charac-

teristic peaks of LaOF on the wear marks resulting from friction at 800 °C. Furthermore, at 800 °C, only $LaCrO_3$ is detectable in the XRD of the wear scar area. Simultaneously, a faint characteristic peak of NiO appeared in the Raman spectrum, indicating that NiO is also a component of the composite oxide film. This suggests that the oxidation of the friction surface is more extensive compared to the non-friction region, with a predominant accumulation of oxides on the wear mark surface.

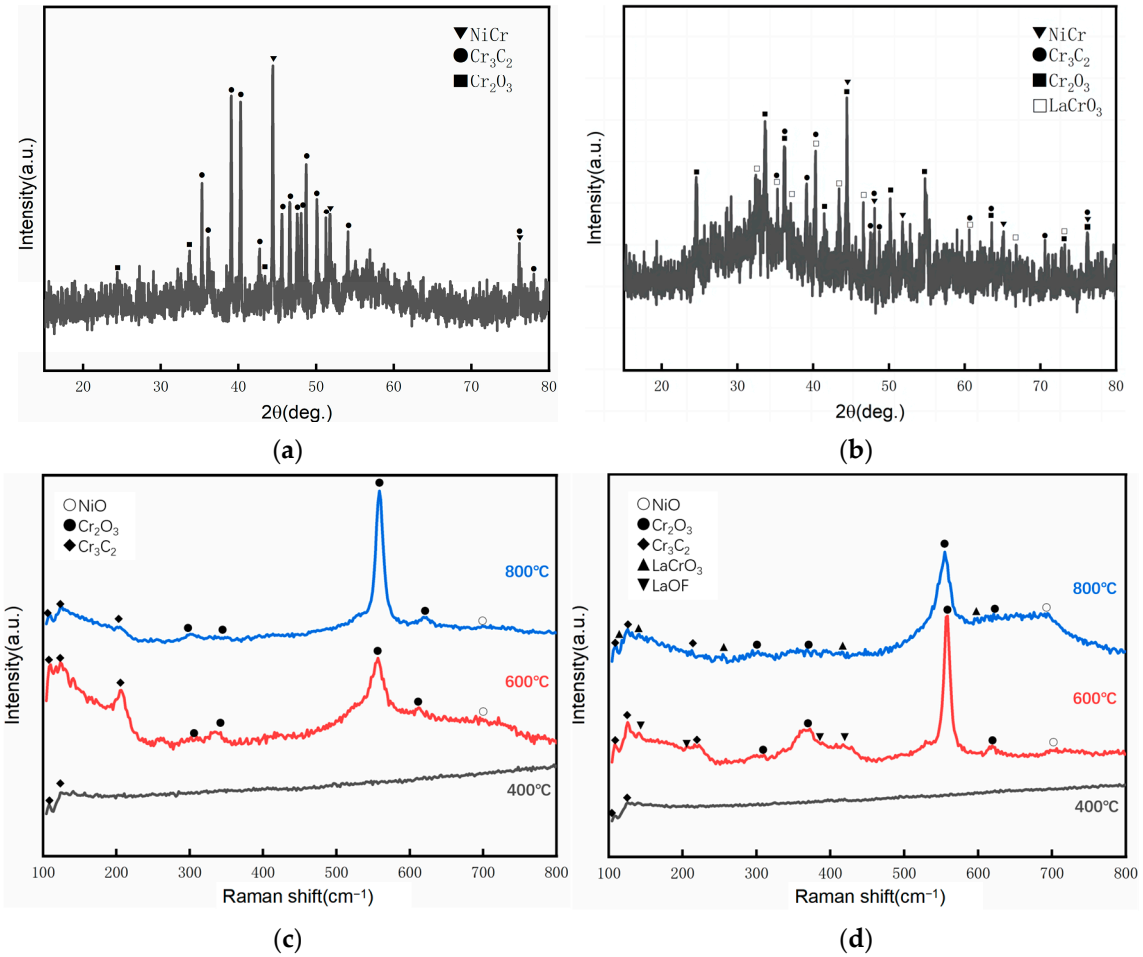

Figure 12. XRD patterns of the worn surface of NCL0 (**a**) and NCL20 (**b**) at 800 °C; Raman spectra of worn surface of NCL0 (**c**) and NCL20 (**d**) at 400 °C, 600 °C, and 800 °C.

3.4. Lubricating and Wear Mechanism

Due to its unique shearable and layered hexagonal structure, the incorporation of LaF_3 serves to effectively decrease the coefficient of friction exhibited by the material. As ambient temperatures increase, LaF_3 accumulates on the material's surface, forming a protective transfer film. However, under elevated temperature conditions, particularly at 600 °C, LaF_3 and Cr_3C_2 undergo distinct oxidation reactions within the material matrix. Notably, LaF_3 and Cr_3C_2 are typically combined during the sintering process; hence, the oxidation of these constituent components leads to the detachment of Cr_3C_2 hard particles from the material's surface. In contrast, at temperatures reaching 800 °C, LaF_3 and Cr_3C_2 undergo favorable tribochemical reactions, culminating in the formation of $LaCrO_3$. This reaction is accompanied by a series of processes including crushing, stacking, compaction, and subsequent re-sintering [34]. Consequently, this reactive process results in the development of a surface layer enriched with $LaCrO_3$, NiO, and Cr_2O_3. This layer significantly reduces frictional resistance and effectively mitigates material degradation, thereby enhancing the overall performance and durability of the material system. This process is shown in Figure 13.

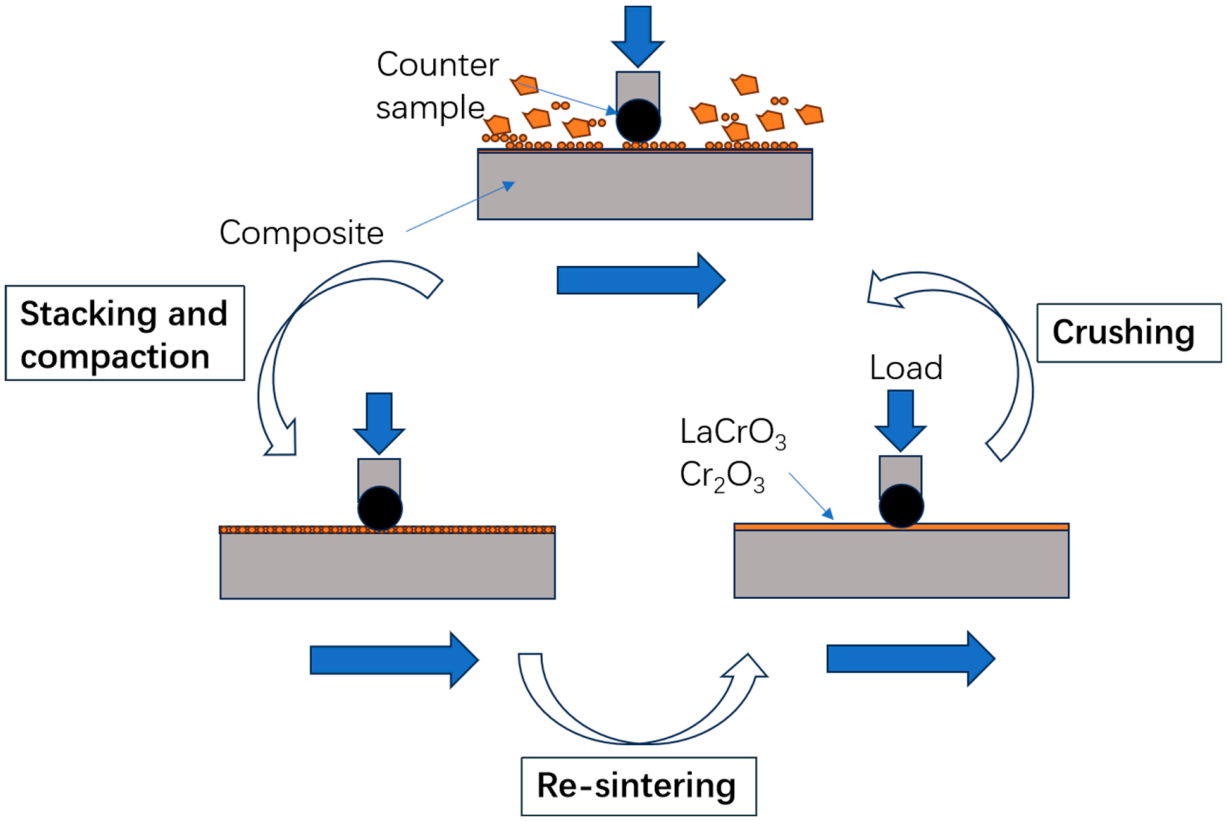

Figure 13. Schematic diagram of 800 °C friction lubrication mechanism.

4. Conclusions

(1) The NiCr/Cr_3C_2-LaF_3 composites were successfully fabricated through fast hot pressing sintering techniques, exhibiting remarkable density and hardness.
(2) These composites demonstrated excellent friction properties across the tested temperature range, with NCL15 exhibiting superior comprehensive properties, including a ceramic phase hardness of 1412 HV, a friction coefficient ranging from 0.74 to 0.4, and wear rates varying from 4.46×10^{-6} to 5.72×10^{-5} $mm^3N^{-1}m^{-1}$.
(3) The friction behavior analysis of the NCL series composites demonstrated that LaF_3 effectively lubricates at different temperatures and forms a unique lubricating phase with Cr_3O_2 at higher temperatures. However, at 600 degrees Celsius, the formation of LaOF from LaF_3 results in a deterioration of friction performance.

Author Contributions: Conceptualization, W.Z. and C.H.; methodology, H.Y. and H.Z.; validation, H.Y., Y.L. and Y.S.; investigation, H.Y., Y.L. and Y.W.; formal analysis, H.L. (Haozhong Lv), Y.W. and Y.S.; resources, C.H. and H.L. (Hao Lan);writing—original draft preparation, H.Y.; data curation: H.Y. and Y.W.; writing—review and editing, C.H., H.L. (Haozhong Lv) and H.Z.; supervision, W.Z., C.H. and H.L. (Hao Lan); funding acquisition, W.Z. and C.H. All authors have read and agreed to the published version of the manuscript.

Funding: This research is sponsored by Self-deployed Projects of Ganjiang Innovation Academy, Chinese Academy of Sciences [grant number E155D001]; The Key Research Program of the Chinese Academy of Sciences [grant numbers ZDRW-CN-2021-2-2 and ZDRW-CN-2021-2-1-3]; Projects of the Innovation Academy for Green Manufacture, Chinese Academy of Sciences [grant number IAGM 2020DB04]; Double Thousand Plan of Jiangxi Province [grant number jxsq2020105012].

Data Availability Statement: Data are contained within the article.

Conflicts of Interest: The authors declare that they have no known competing financial interests or personal relationships that could have appeared to influence the work reported in this paper.

References

1. John, M.; Menezes, P.L. Self-Lubricating Materials for Extreme Condition Applications. *Materials* **2021**, *14*, 5588. [CrossRef] [PubMed]
2. Mazumder, S.; Metselaar, H.S.C.; Sukiman, N.L.; Zulkifli, N.W.M. An overview of fluoride-based solid lubricants in sliding contacts. *J. Eur. Ceram. Soc.* **2020**, *40*, 4974–4996.
3. Torres, H.; Ripoll, M.R.; Prakash, B. Tribological behaviour of self-lubricating materials at high temperatures. *Int. Mater. Rev.* **2017**, *63*, 309–340. [CrossRef]
4. Cui, G.; Liu, H.; Li, S.; Gao, G.; Kou, Z. Design and high-temperature tribological properties of CoCrW with rare earth fluoride composites. *J. Mater. Res. Technol.* **2020**, *9*, 2402–2411.
5. Cui, G.; Qian, Y.; Bian, C.; Gao, G.; Hassani, M.; Liu, Y.; Kou, Z. CoCrNi matrix high-temperature wear resistant composites with micro- and nano-Al_2O_3 reinforcement. *Compos. Commun.* **2020**, *22*, 100461. [CrossRef]
6. Wang, Y.; Liu, X.-B.; Liu, Y.-F.; Luo, Y.-S.; Meng, Y. Microstructure and tribological performance of Ni60-based composite coatings on Ti6Al4V alloy with different Ti_3SiC_2 ceramic additions by laser cladding. *Ceram. Int.* **2020**, *46*, 28996–29010. [CrossRef]
7. Xu, J.; Kong, X.; Chen, M.; Wang, Q.; Wang, F. High-entropy FeNiCoCr alloys with improved mechanical and tribological properties by tailoring composition and controlling oxidation. *J. Mater. Sci. Technol.* **2021**, *82*, 207–213. [CrossRef]
8. Duran, C.; Eroglu, S. Liquid phase sintering and properties of Cr_3C_2/NiCr cermets. *J. Mater. Process. Technol.* **1998**, *74*, 69–73. [CrossRef]
9. Alroy, R.J.; Kamaraj, M.; Lakshmi, D.V.; Praveen, K.; Babu, P.S.; Sivakumar, G. Tailoring microstructural features of Cr_3C_2-25NiCr coatings through diverse spray variants and understanding the high-temperature erosion behavior. *Tribol. Int.* **2023**, *188*, 108810. [CrossRef]
10. Zhang, C.; Ma, H.; Bao, C. Corrosive Wear Mechanism of Supersonic Atmospheric Plasma Spray Coating of Hydraulic Supports in Industrial Environment. *J. Mater. Eng. Perform.* **2024**, 1–11. [CrossRef]
11. Hu, G.; Han, Y.; Liu, S.; Yu, B.; Tang, W.; Li, D.; Xing, H.; Liu, X.; Zhang, J.; Sun, B. In-situ crystalline Cr_3C_2 and amorphous SiO_2 dual-particles reinforced NiCr-based composites. *Mater. Des.* **2023**, *230*, 111997. [CrossRef]
12. Yang, X.; Jia, J.; Chen, W.; Yang, G.; Xin, H.; He, N.; Ma, S. Corrosive wear behavior of HVOF-sprayed micro-nano-structured Cr_3C_2–NiCr cermet coatings under aqueous media. *Ceram. Int.* **2022**, *48*, 15144–15151. [CrossRef]
13. Huang, C.; Du, L.; Zhang, W. Effects of solid lubricant content on the microstructure and properties of NiCr/Cr_3C_2–BaF_2·CaF_2 composite coatings. *J. Alloys Compd.* **2009**, *479*, 777–784. [CrossRef]
14. Sliney, H.E.; Strom, T.N.; Allen, G.P. Fluoride solid lubricants for extreme temperatures and corrosive environment in NASA-TM-X-52077. *ASLE Trans.* **1965**, *8*, 307–322. [CrossRef]
15. Deadmore, D.L.; Sliney, H.E. Characterization of the Tribological Coating Composition 77wt% CaF_2-23wt% LiF Fused to IN-750 Alloy. In *NASA-TM-87342*; NASA: Washington, DC, USA, 1986.
16. Deadmore, D.L.; Sliney, H.E. Hardness of CaF_2 and BaF_2 Solid Lubricants at 25 to 670 °C. In *NASA-TM-88979*; NASA: Washington, DC, USA, 1987.
17. Zhao, H.; Luo, L.; Guo, F.; Zhao, X.; Xiao, P. High-temperature tribological behavior of Mo and BaF_2 added Cr_3C_2-NiCr matrix composite. *Ind. Lubr. Tribol.* **2019**, *72*, 136–145. [CrossRef]
18. Kotkowiak, M.; Piasecki, A. Characterization of Wear Properties of Pure Nickel Modified by Ni-Cr Composite and CaF_2 Solid Lubricant Addition. *Materials* **2022**, *15*, 7511. [CrossRef] [PubMed]
19. Su, W.; Zhang, J.; Zhang, J.; Zhou, K.; Niu, S.; Liu, M.; Dai, H.; Deng, C. Microstructure of HVOF-sprayed Ag–BaF_2·CaF_2–Cr_3C_2–NiCr coating and its tribological behavior in a wide temperature range (25 °C to 800 °C). *Ceram. Int.* **2021**, *47*, 865–876. [CrossRef]
20. Sliney, H.E. Rare Earth Fluorides and Oxides: An Exploratory Study of Their Use as Solid Lubricants at Temperature to 1800 °F (1000 °C). In *NASA-TN-D-5301*; NASA: Washington, DC, USA, 1969.
21. Lu, J.; Xue, Q.; Wang, J.; Ouyang, J. The effect of CeF_3 on the mechanical and tribological properties of Ni-based alloy. *Tribol. Nternational* **1997**, *30*, 659–662. [CrossRef]
22. Ren, Q.; Cui, G.; Li, T.; Hassani, M.; Liu, Y.; Kou, Z. High-Temperature Wear Behavior of Cobalt Matrix Composites Reinforced by LaF_3 and CeO_2. *Tribol. Lett.* **2021**, *69*, 149. [CrossRef]
23. Jia, Y.; Wan, H.; Chen, L.; Zhou, H.; Chen, J. Effects of nano-LaF_3 on the friction and wear behaviors of PTFE-based bonded solid lubricating coatings under different lubrication conditions. *Appl. Surf. Sci.* **2016**, *382*, 73–79. [CrossRef]
24. Xie, T.; Shi, Y. Effects of LaF_3/CeF_3 on the friction transfer of PTFE-based composites. *Tribol. Int.* **2021**, *161*, 107069. [CrossRef]
25. Hahn, K.H.; Vedula, K. Room temperature tensile ductility in polycrystalline B_2 NiAl. *Scr. Metall.* **1989**, *23*, 7–12. [CrossRef]
26. Liao, X.; Zhao, L.; Zhang, J.; Ahmed, G.; Khan, A.; Zeng, H.; Yu, H.; Zhong, X.; Liu, Z.; Zhang, G. Clarifying the basic phase structure and magnetic behavior of directly quenched $(Ce,La)_2Fe_{14}B$ alloys with various Ce/La ratios. *Curr. Appl. Phys.* **2019**, *19*, 733–738. [CrossRef]
27. Chu, R.; Fan, Y.; Li, Z.; Liu, J.; Yin, N.; Hao, N. Study on the Control of Rare Earth Metals and Their Behaviors in the Industrial Practical Production of Q420q Structural Bridge Steel Plate. *Metals* **2018**, *8*, 240. [CrossRef]
28. Li, J.; Lu, W. Effects of AlN and rare earth fluorides on the thermal conductivity of SiC ceramics with impedance spectroscopy analysis. *J. Phys. Conf. Ser.* **2021**, *2011*, 012054. [CrossRef]

29. Wu, R.; Huang, C.; Zhang, H.; Lv, H.; Sun, X.; Lan, H.; Zhang, W. Microstructure and High-Temperature Ablation Behaviour of Hafnium-Doped Tungsten-Yttrium Alloys. *Materials* **2023**, *16*, 2529. [CrossRef]
30. Li, H.; Zhou, M.; Tian, B.; Zhang, Y.; Ma, Z.; Li, X.; Zou, J.; Hu, H.; Jing, K.; Liu, Y.; et al. Microstructure and electrical contact properties of Al_2O_3-Cu/(Cr, Zr) composites. *Mater. Today Commun.* **2024**, *38*, 107747. [CrossRef]
31. Zhu, H.; Zhou, M.; Jing, K.; Tian, B.; Zhang, Y.; Li, X.; Li, Y.; Zheng, X.; Li, H.; Ma, Z.; et al. Hot deformation behavior of $0.5Y_2O_3/AlO_2$-Cu/$30Mo_3SiC$ composites doped with reduced graphene oxide. *J. Mater. Res. Technol.* **2023**, *26*, 7444–7459. [CrossRef]
32. Zhu, B.; Chen, N.; Zhu, D.; Li, Y.; Sun, W.; Liu, G.; Du, G. Thermal annealing of LaF_3:Eu3+ nanocrystals synthesized by a solvothermal method and their luminescence properties. *J. Sol-Gel Sci. Technol.* **2013**, *66*, 126–132. [CrossRef]
33. Tan, X.; Zhao, Z.; Wang, N.; Zhang, Z.; Wang, X.; Feng, Z.; Zheng, Y.; Yang, J.; Huang, X. Phase transition process and mechanism of LaOF in air: From experiment to theory. *Ceram. Int.* **2023**, *49*, 40659–40667. [CrossRef]
34. Inman, I.; Datta, S.; Du, H.; Burnell-Gray, J.; Luo, Q. Microscopy of glazed layers formed during high temperature sliding wear at 750 °C. *Wear* **2003**, *254*, 461–467. [CrossRef]